Electronic Supplementary Material (ESI) for Journal of Materials Chemistry A.


# Supporting Information

## Migration of Cations in Layered Oxides for Creating Highly Active Interface toward CO Preferential Oxidation

*Junfang Ding[†], Zhibin Geng[†], Liping Li[†], Ye Wang[†], Ying Zuo[‡], Huixia, Li[†], Min Yang[†], and Guangshe Li*[,†]*

[†]State Key Laboratory of Inorganic Synthesis and Preparative Chemistry, College of Chemistry, Jilin University, Changchun 130012, P.R. China

[‡]Scientific Instrument Center, Shanxi University, Shanxi 030006, P.R. China

*E-mail: guangshe@jlu.edu.cn.

**Table of Contents**

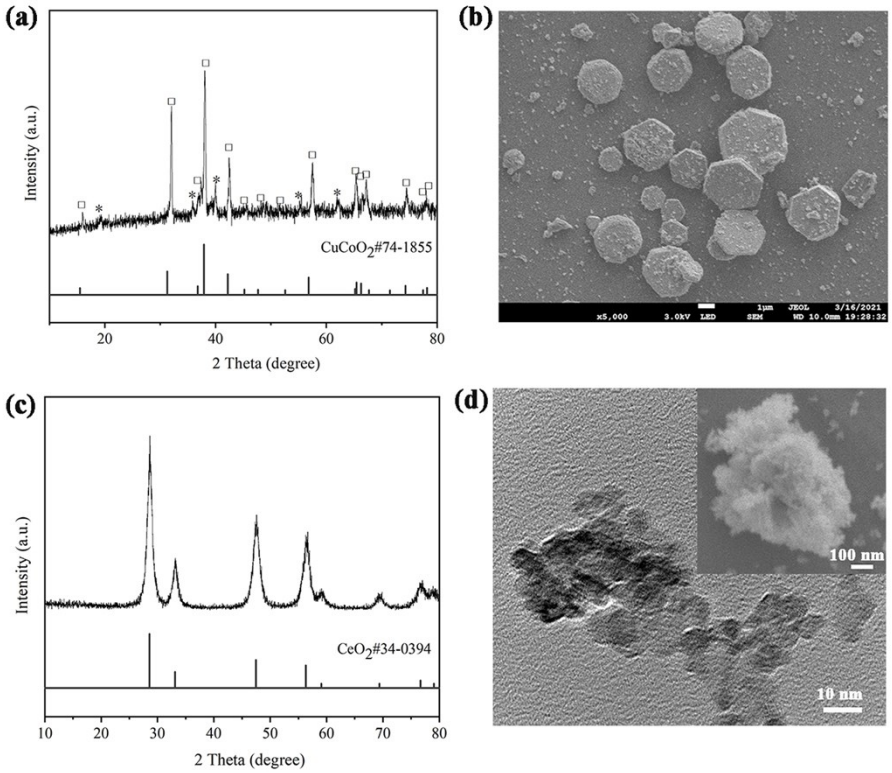


**Figure S1** XRD patterns of the precursors $CuCoO_2$ (a) and $CeO_2$ (c); SEM image of $CuCoO_2$ (b); and TEM image of $CeO_2$ (d). Inset is SEM image of $CeO_2$.

As shown in Figure S1a, the synthesized precursors contain the majority of rhombohedral (3R) delafossite $CuCoO_2$ phase (indicated as an open square) and small amount of un-known impurity phase (an asterisk). The diffraction peaks at two theta of 28.6$^o$, 33.2$^o$, 47.5$^o$, and 56.7$^o$ are attributed to the planes (111), (002), (022), and (113) of $CeO_2$ in a cubic fluorite structure, respectively. $CuCoO_2$ mainly composed of hexagonal plates and fragmented particles. The morphology of $CeO_2$ is rough spherical at a diameter about 6-7 nm, which agrees with the XRD data analysis.

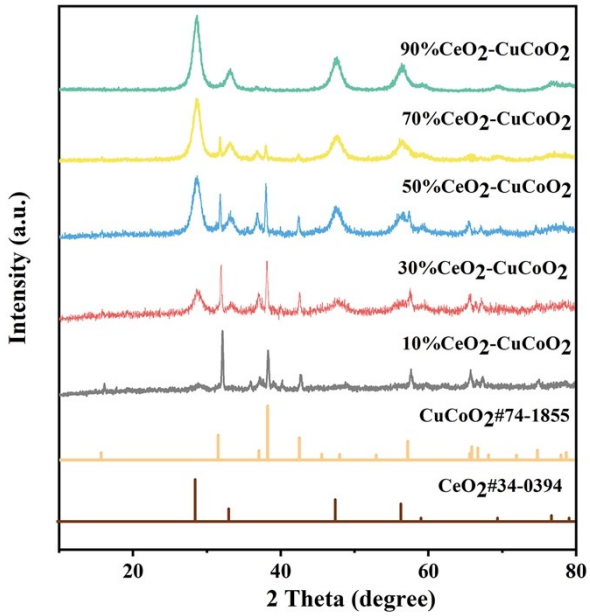


**Figure S2** XRD patterns of the given samples along with the standard diffraction data for $CeO_2$ (JCPDS No. 34-0394) and for $CuCoO_2$ (JCPDS No. 74-1855).

For 10% $CeO_2$-$CuCoO_2$ sample as shown in Figure S2, the diffraction peaks were substantially the same as the precursors, except for both weak peaks at 2θ of 28.554° and 47.478° that are attributed to (111) and (220) crystalline planes of cubic-phase $CeO_2$ (JCPDS No. 34-0394), confirming that 10% $CeO_2$-$CuCoO_2$ is mainly composed of $CuCoO_2$ with a small amount of $CeO_2$. In XRD patterns of 30% $CeO_2$-$CuCoO_2$ and 50% $CeO_2$-$CuCoO_2$, the intensities of the characteristic peaks of cubic-phase $CeO_2$ became stronger with the appearance of the peak located at 56.085° assigned to (222) crystalline planes of cubic-phase $CeO_2$, corresponding to the higher mass fraction of $CeO_2$ in the as-prepared catalysts. When the content of $CeO_2$ grew higher to 70%, it can be clearly seen that the intensities of $CuCoO_2$ characteristic peaks suffered a sharp decline. In the XRD patterns of 90% $CeO_2$-$CuCoO_2$, peaks of $CuCoO_2$ were almost invisible, demonstrating the extremely low content of $CuCoO_2$.

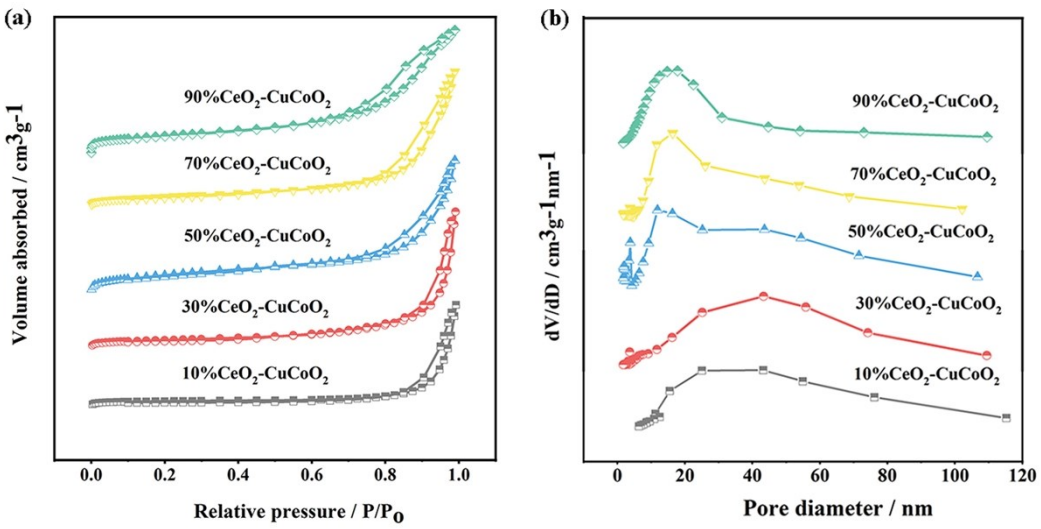


**Figure S3** (a) $N_2$ adsorption-desorption isotherms and (b) pore size distributions of samples.

The specific surface area and the corresponding Barrett-Joyner-Halenda (BJH) pore size distributions of the as-prepared samples were investigated by $N_2$ adsorption-desorption isotherms. As shown in Figure S3, all samples exhibited IV type isotherms with a H3 representative hysteresis loop, suggesting that the pores were mainly caused by the accumulation of small nanoparticles. From Table 1, it can be seen that with the increase of $CeO_2$ content, the surface areas of samples increase gradually. This observation can be explained in terms of a small size effect because the particle size of $CeO_2$ component is only about 6 nm. Meanwhile, BJH pore volume is also enhanced with $CeO_2$ content, and it is summarized in Table 1. The pore size distribution calculated from the desorption branch of the samples is presented in Figure 3b. The samples of 10%$CeO_2$-$CuCoO_2$ and 30%$CeO_2$-$CuCoO_2$ were mainly mesopores located at about 20-40 nm which was formed from the surface wall. The peaks of mesopore size distribution of 50%$CeO_2$-$CuCoO_2$, 70%$CeO_2$-$CuCoO_2$ and 90%$CeO_2$-$CuCoO_2$ shifted toward smaller pore width when compared with above two samples, which was due to the fact that the content of $CeO_2$ increased slightly and crystal grains of $CeO_2$ is much smaller than $CuCoO_2$. This observation is in good agreement with adsorption-desorption isotherms, SEM and TEM results.

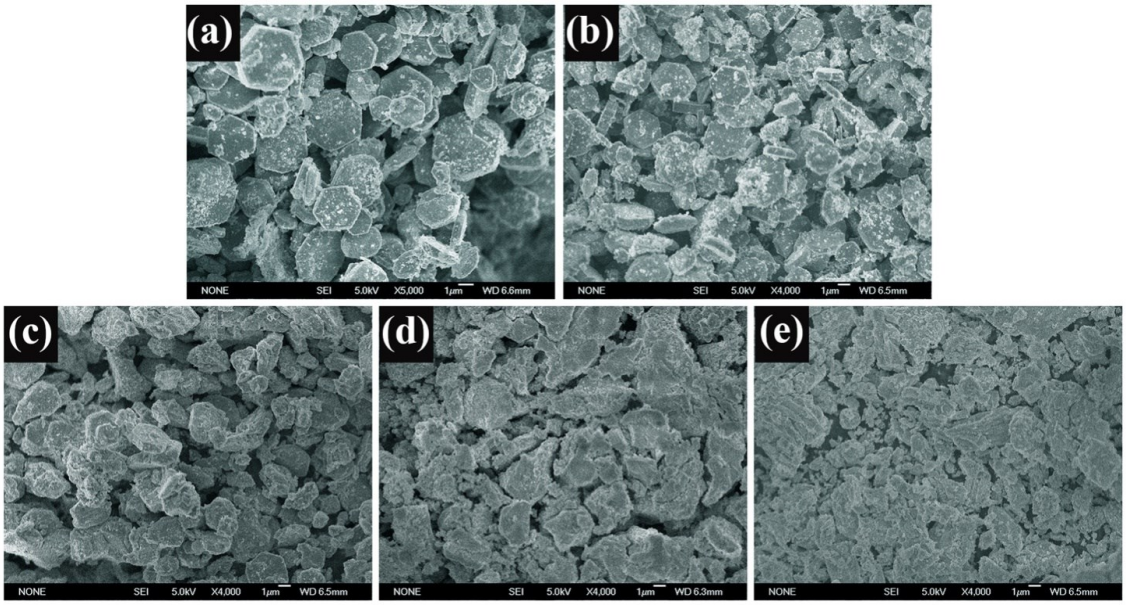


**Figure S4** SEM images of the samples: (a) 10%$CeO_2$-$CuCoO_2$; (b) 30%$CeO_2$-$CuCoO_2$; (c) 50%$CeO_2$-$CuCoO_2$; (d) 70%$CeO_2$-$CuCoO_2$; and (e) 90%$CeO_2$-$CuCoO_2$.

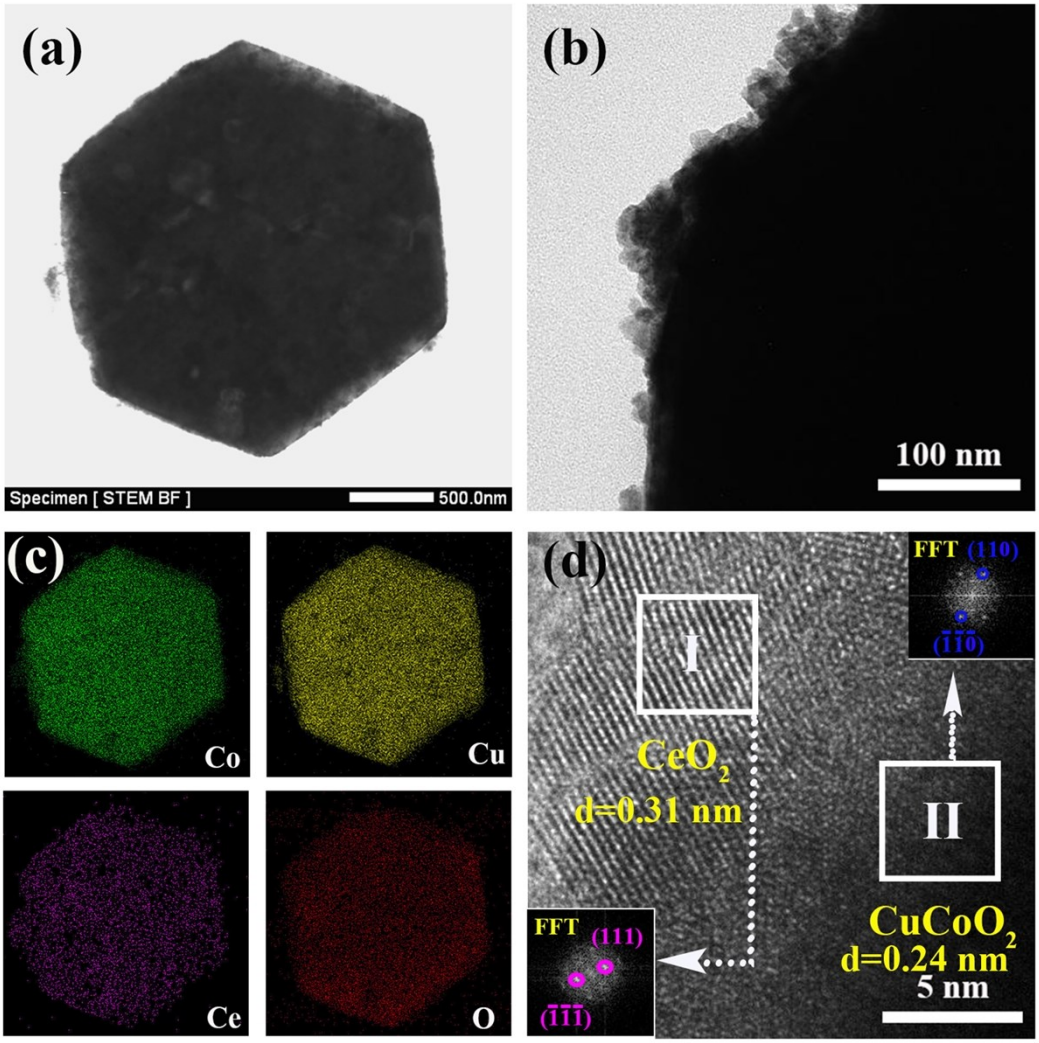


**Figure S5.** (a) TEM image, (b) enlarged images of Figure a, (c) corresponding elemental mapping analysis in the area of (a), and HRTEM image of 10%$CeO_2$-$CuCoO_2$.

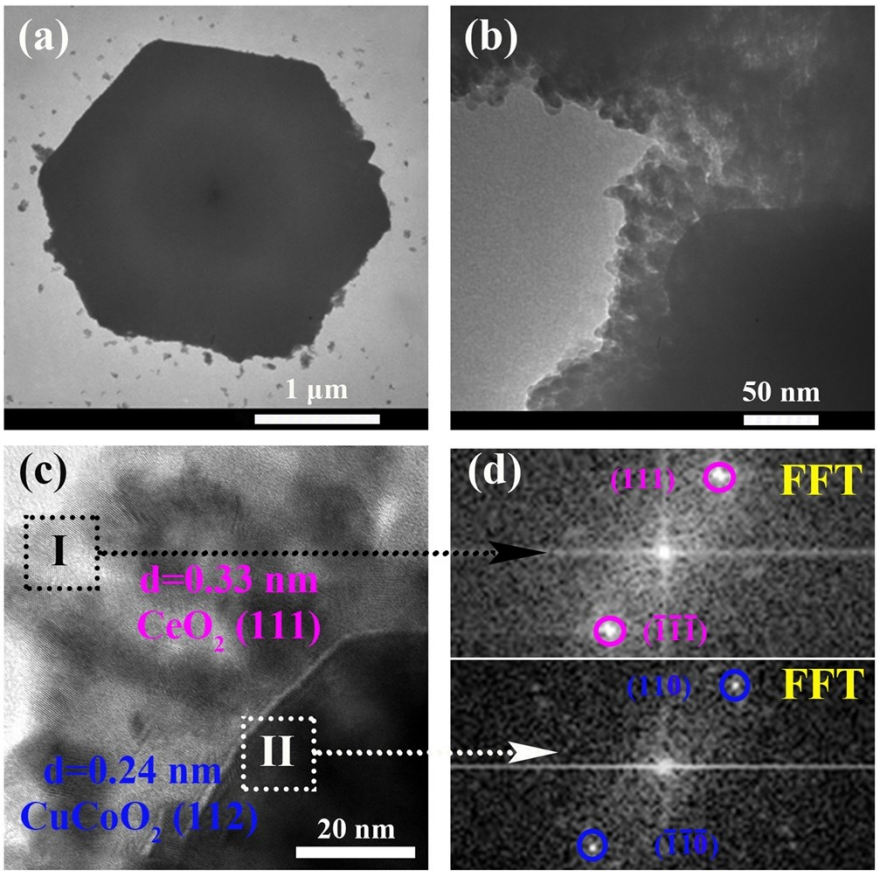


**Figure S6.** (a) TEM image, (b) enlarged images of Figure a, (c) HRTEM image, and FFT pattern in the rectangle region I, II of (c) for 30%$CeO_2$-$CuCoO_2$.

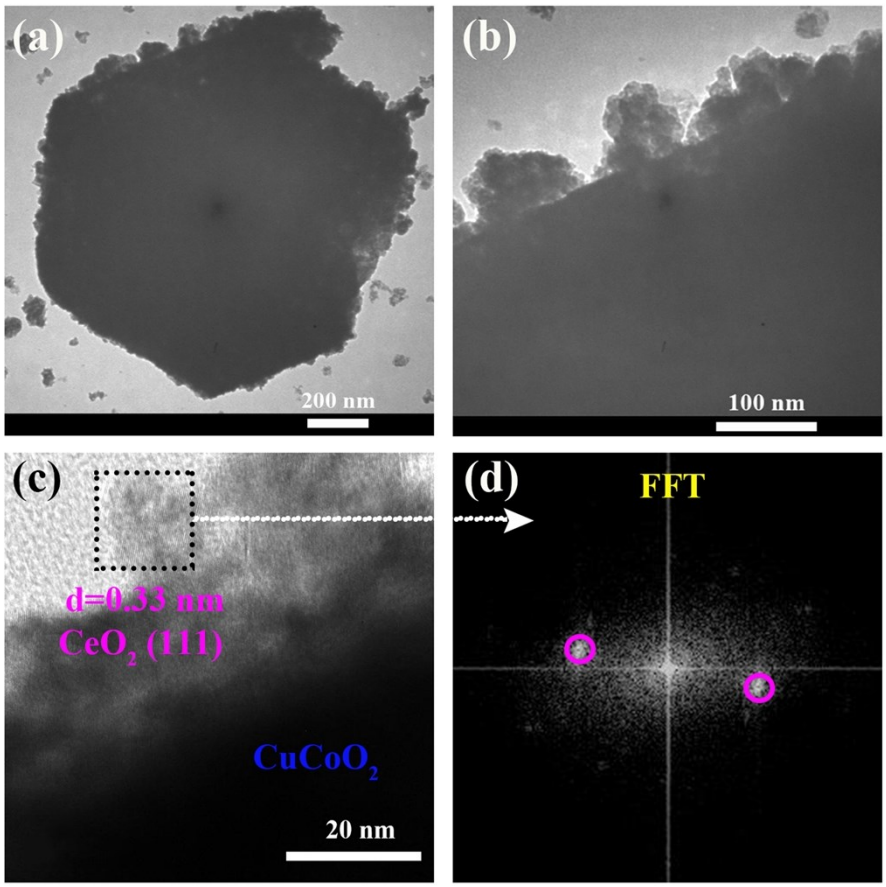


**Figure S7.** (a) TEM image, (b) enlarged images of Figure a, (c) HRTEM image, and FFT pattern in the rectangle region I of (c) for 50%$CeO_2$-$CuCoO_2$.

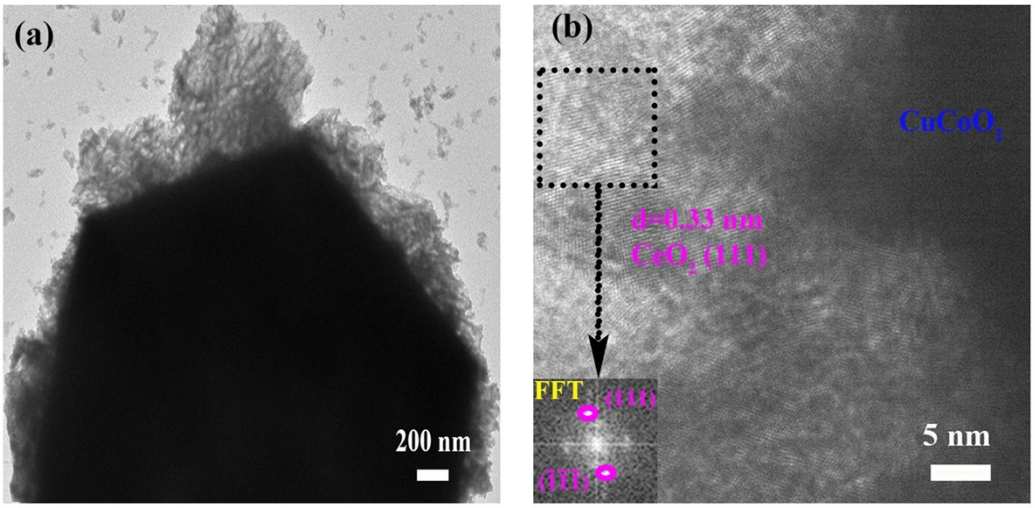


**Figure S8** (a) TEM image, and (b) HRTEM image of 90%$CeO_2$-$CuCoO_2$, FFT pattern in the rectangle region.

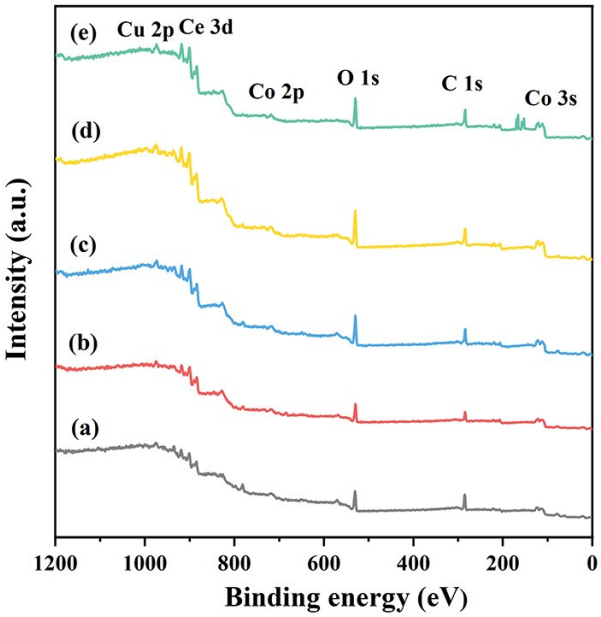


**Figure S9** XPS survey scans of the samples: (a) 10%$CeO_2$-$CuCoO_2$;(b) 30%$CeO_2$-$CuCoO_2$; (c) 50%$CeO_2$-$CuCoO_2$; (d) 70%$CeO_2$-$CuCoO_2$; and (e) 90%$CeO_2$-$CuCoO_2$.

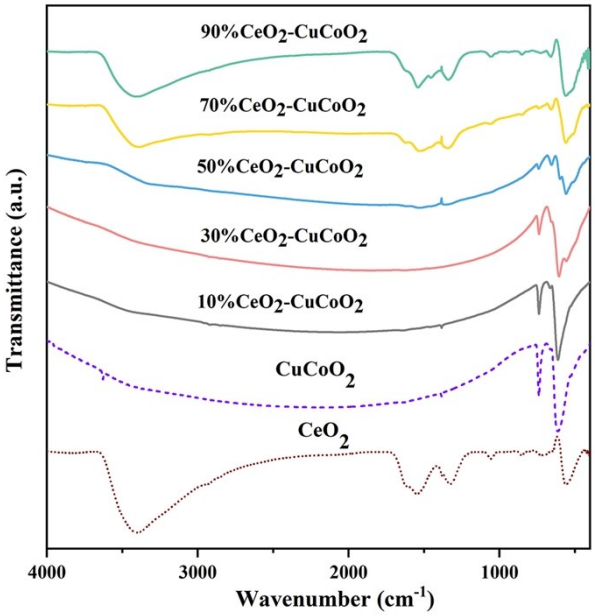


**Figure S10** FT-IR spectra for all samples.

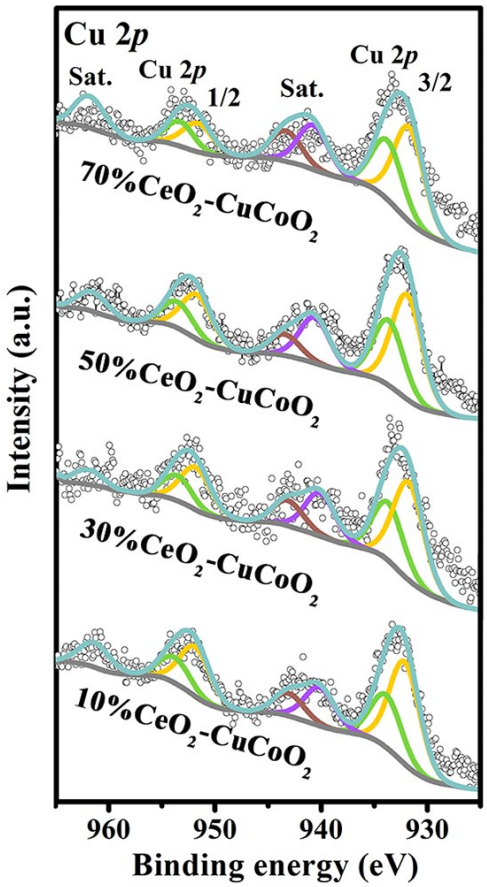


**Figure S11** XPS spectra of the Cu 2*p* for samples.

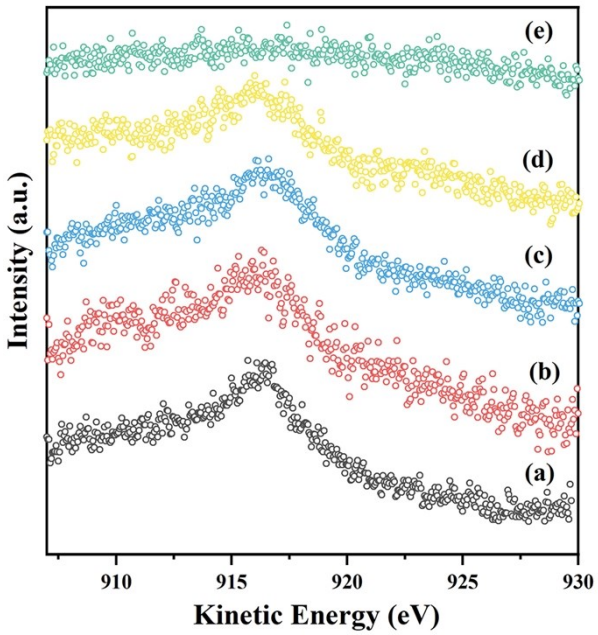


**Figure S12** Auger spectra (Cu LMM peak) of the samples: (a) 10%$CeO_2$-$CuCoO_2$; (b) 30%$CeO_2$-$CuCoO_2$; (c) 50%$CeO_2$-$CuCoO_2$; (d) 70%$CeO_2$-$CuCoO_2$; and (e) 90%$CeO_2$-$CuCoO_2$.

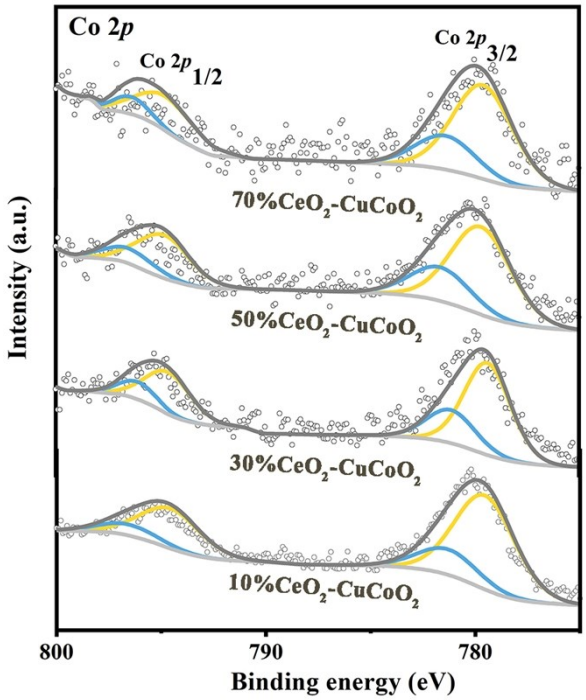


**Figure S13** XPS spectra of the Co 2*p* for samples.

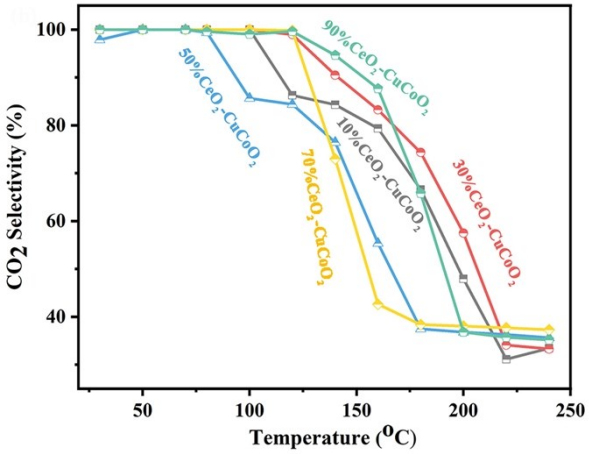


**Figure S14** $CO_2$ selectivity for the samples with varied $CeO_2$ content.

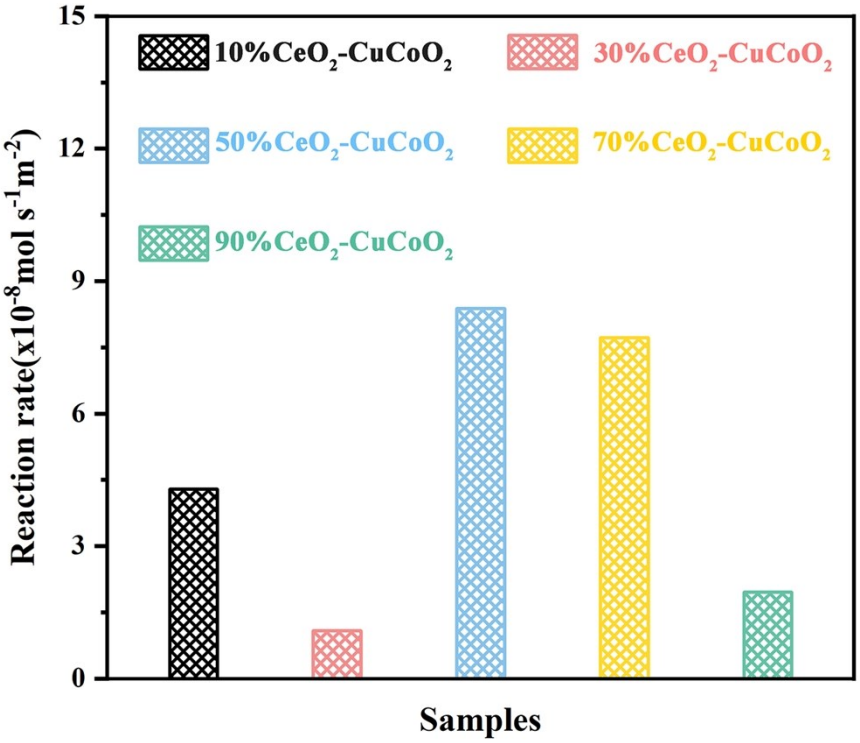


**Figure S15** Reaction rates of the samples under CO-PROX conditions at 100 °C.

**Table S1** Comparison of catalytic performance in CO-PROX over 70%$CeO_2$-$CuCoO_2$ and those catalysts reported in literatures.

| Sample | Amount of catalyst (mg) | Space Velocity ($ml \cdot g_{cat}^{-1} \cdot h^{-1}$) | Feed gas | operation temperature window (CO conversion >95.0%) | Ref |
|---|---|---|---|---|---|
| 70%$CeO_2$-$CuCoO_2$ | 50 | 60 000 | 1% CO, 1.25% $O_2$, 50% $H_2$, He balance | 120-240 °C | This work |
| $Co_{2.6}Zn_{0.4}O_4/Al_2O_3$ -gly | 150 | 40 000 | 2% CO, 2% $O_2$, 30% $H_2$, He balance | 200-225 | 1 |
| Co-CuCZ | 300 | 24 000 | 1 % CO, 1 % $O_2$, 50 % $H_2$, He balance | 100-160 °C | 2 |
| CuCe-Fe | 300 | 16 000 | 1 % CO, 1 % $O_2$, 50 % $H_2$, He balance | 100-180 °C | 3 |
| 40%$CeO_2$/ $CuMn_2O_4$ | Undefined | 80 000 | 1% CO, 1.25% $O_2$, 50% $H_2$, 0.2% $H_2O$, He balance | 175-200 °C | 4 |
| 80%$CeO_2$/ $CuMn_2O_4$ | Undefined | 80 000 | 1% CO, 1.25% $O_2$, 50% $H_2$, 0.2% $H_2O$, He balance | 175-200 °C | 4 |
| CuCoCe30 | 500 | 12 000 | 1 % CO, 1 % $O_2$, 50% $H_2$, balance $N_2$ | 126-189 °C | 5 |
| CoCuCe | 100 | 12 000 | 1% CO, 1% $O_2$, 60% $H_2$, balance He | 140-200 °C | 6 |
| 1/10$Fe_{(N)}$-CuCZ. | 300 | 24 000 | 1% CO, 1% $O_2$, 50% $H_2$, balance He | 100-160 °C | 7 |
| $CoFe_2O_4$ | 150 | 40 000 | 1% CO, 1% $O_2$, 60% $H_2$, balance He | ---- | 8 |
| 10COCE | 150 | 22 000 | 1.25 % CO, 1.25 % $O_2$, 50 % $H_2$, He balance | 140-190 °C | 9 |
| CuNiCeO | 150 | 40 000 | 1 % CO, 1 % $O_2$, 60% $H_2$, balance He | 125-150 °C | 10 |
| $Ce_{0.87}Cu_{0.03}Co_{0.10}O_{2-\delta}$ | Undefined | 48 000 | 1 % CO, 1 % $O_2$, 50% $H_2$, balance $N_2$ | 180-250 °C | 11 |
| $CeO_2$-$Co_3O_4$/CuO (CAT-350) | Undefined | 40 000 | 1 % CO, 1 % $O_2$, 50% $H_2$, balance $N_2$ | 145-225 °C | 12 |
| FCZCu77 | Undefined | 22 000 | 1.25 % CO, 1.25 % $O_2$, 50 % $H_2$, He balance | 115-165 °C | 13 |
| Co-Mn-O-np | 100 | 15 000 | 1 % CO, 1 % $O_2$, 50% $H_2$, balance Ar | 150-225 °C | 14 |
| 30%Co/$CeO_2$ | 200 | 15 000 | 1 % CO, 1 % $O_2$, 50% $H_2$, balance Ar | 150-225 °C | 15 |

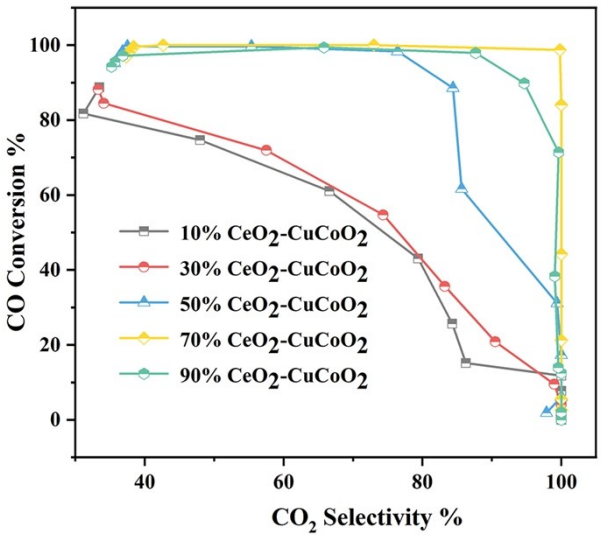


**Figure S16** Selectivity to $CO_2$ as a function of CO conversion for given samples.

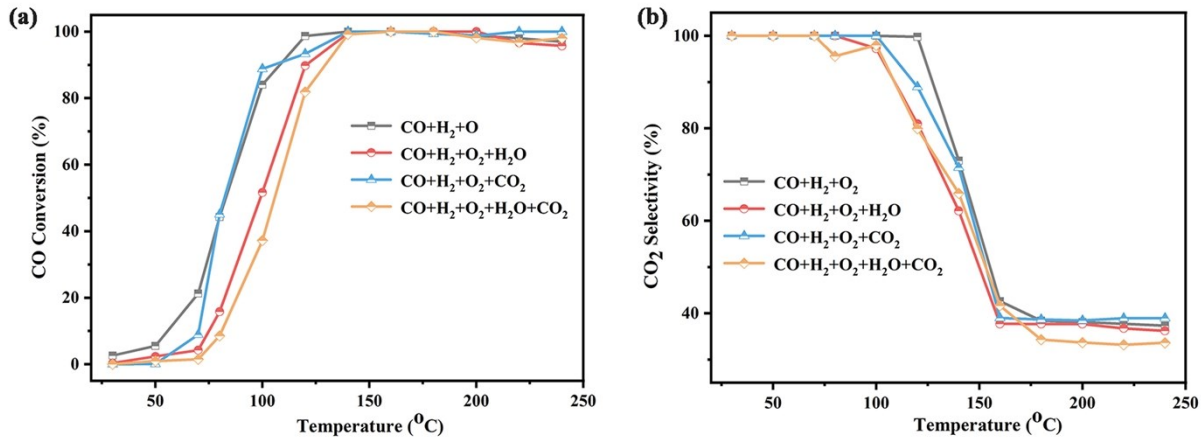


**Figure S17** CO conversion (a) and $CO_2$ selectivity (b) of 70%$CeO_2$-$CuCoO_2$ sample in the presence of $CO_2$ and $H_2O$.

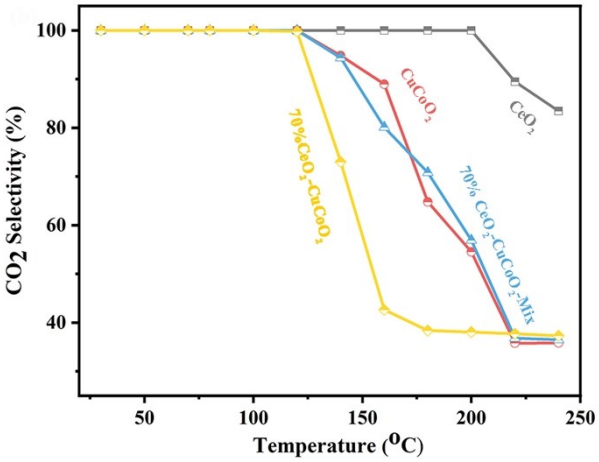


**Figure S18** $CO_2$ selectivity for given samples.

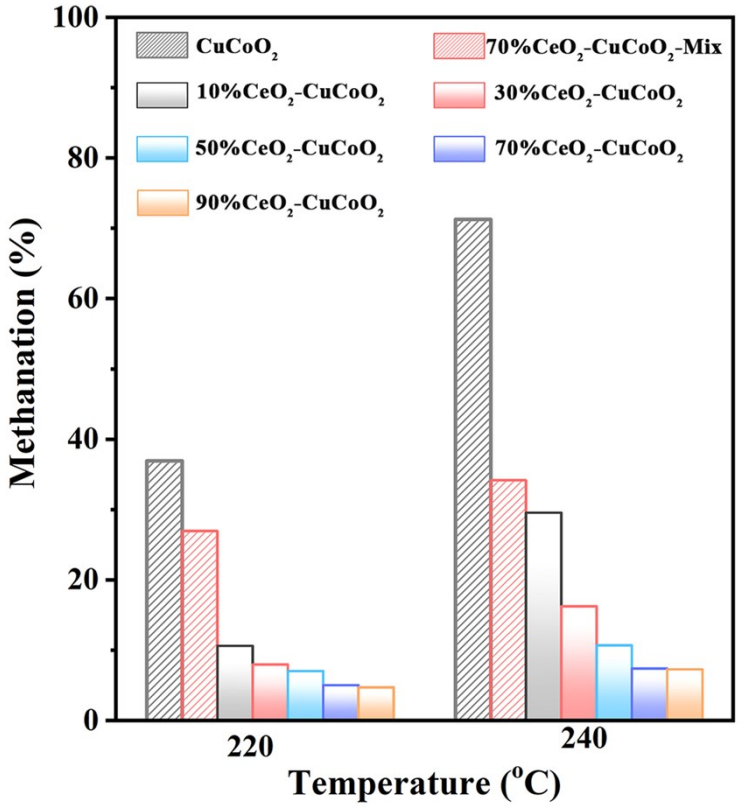


**Figure S19** $CO_2$ (CO) methanation over the given samples at 220 °C and 240 °C.

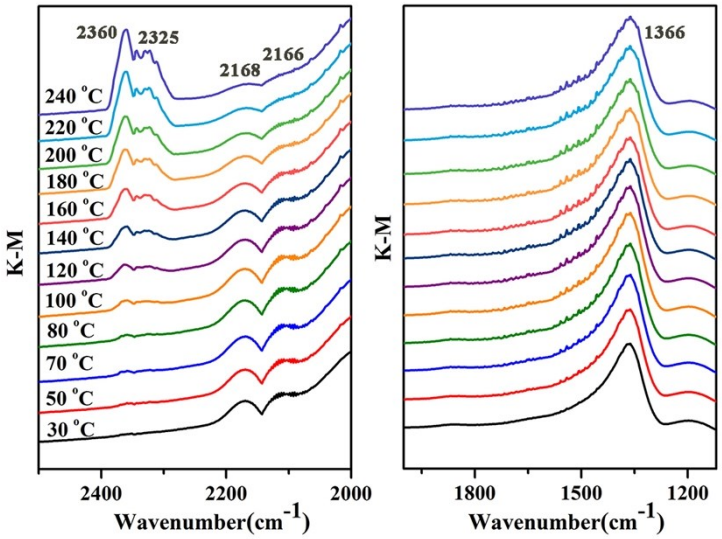


**Figure S20** DRIFTS spectra obtained for sample 50%$CeO_2$-$CuCoO_2$ at given temperatures under CO-PROX conditions (1% CO, 1.25% $O_2$ and 50% $H_2$ in He).

## References:


1. G. Grzybek, K. Ciura, J. Gryboś, P. Indyka, A. Davó-Quiñonero, D. Lozano-Castelló, A. Bueno-Lopez, A. Kotarba, and Z. Sojka, *J Phys Chem C.*, 2019, **123**, 20221-20232.

2. J. Lu, J. Wang, Q. Zou, Y. Zhao, J. Fang, S. He, D. He and Y. Luo, *J. Alloys Comp.*, 2019, **784**, 1248-1260.

3. J. Lu, J. Wang, Q. Zou, D. He, L. Zhang, Z. Xu, S. He and Y. Luo, *ACS Catal.*, 2019, **9**, 2177-2195.

4. A. Elmhamdi, L. Pascual, K. Nahdi and A. Martínez-Arias, *Appl. Catal. B Environ.*, 2017, **217**, 1-11.

5. Y. Chen, D. Liu, L. Yang, M. Meng, J. Zhang, L. Zheng, S. Chu and T. Hu, *Chem. Eng. J.*, 2013, **234**, 88-98.

6. J. Ayastuy, E. Fernández-Puertas, M. González-Marcos and M. Gutiérrez-Ortiz, *Int. J. Hydrogen Energy.*, 2012, **37**, 7385-7397.

7. J. Wang, C. Han, X. Gao, J. Lu, G. Wan, D. He, R. Chen, K. Chen, S. He and Y. Luo, *J. Power Sources.*, 2017, **343**, 437-445.

8. C. Chagas, E. Souza, M. Carvalho, R. Martins and M. Schmal, *Appl. Catal. A General.*, 2016, **519**, 139-145.

9. A. Arango-Diaz, J. Cecilia, J. Marrero-Jerez, P. Nuñez, J. Jiménez-Jiménez and E. Rodríguez-Castellón, *Ceram. Int.*, 2016, **42**, 7462-7474.

10. C. Chagas, E. Souza, R. Manfro, S. Landi, M. Souza and M. Schmal, *Appl. Catal. B Environ.*, 2016, **182**, 257-265.

11. T. Cwele, N. Mahadevaiah, S. Singh and H. Friedrich, *Appl. Catal. B Environ.*, 2016, **182**, 1-14.

12. S. Zeng, Q. Wang, Y. Wang, Y. Fei, N. Liu, S. Ding and H. Su, *J. Nanosci. Nanotech.*, 2016, **16**, 962-966.

13. E. Moretti, L. Moretti, A. Talon, P. Riello, A. Molina and E. Rodríguez-Castellón, *Appl. Catal. B Environ.*, 2015, **168-169**, 385-395.

14. Z. Zhao, J. Lin and G. Wang, *AIChE J.*, 2015, **61**, 239-252.

15. C. Yan, H. Chen, R. Hu, S. Huang, W. Luo, C. Guo, M. Li and W. Li, *Int. J. Hydrogen Energy.*, 2014, **39**, 18695-18701.